Elucidation of Metal-Sugar Complexes: When Tungstate Combines with D-Mannose

Sabah El Mohammad, Olivier Proux, Antonio Aguilar, Jean-Louis F Hazemann, Christèle Legens, Céline Chizallet, Kim Larmier

Elucidation of Metal-Sugar Complexes: When Tungstate Combines with D-Mannose

Sabah El Mohammad[a], Olivier Proux[b], Antonio Aguilar[c], Jean-Louis Hazemann[d], Christele Legens[a], Céline Chizallet[a] Kim Larmier[a,*]

[a] *IFP Energies nouvelles, Rond-Point de l'Echangeur de Solaize, 69360 Solaize, France.*
[b] *OSUG, UAR 832 CNRS, Université Grenoble Alpes, 38041, Grenoble, France.*
[c] *ICMG, UAR 2607 CNRS, Université Grenoble Alpes, 38041, Grenoble, France.*
[d] *Institut Néel, CNRS, Université Grenoble Alpes, 25 Avenue des Martyrs, 38042 Grenoble, France.*

SYNOPSIS : A combination of spectroscopies and molecular modeling allowed to determine the speciation of tungstate ions in the presence of mannose and its dependence with pH and concentration of species. The speciation shares similarities with that of tungstate ions in mannose-free aqueous solutions, with dominant mononuclear species in basic solutions and dominant oligomeric species in neutral medium, though distinct features exist (existence domain, maximum nuclearity etc.). This paves the way towards mechanistic studies of sugar conversion by such catalytic species.

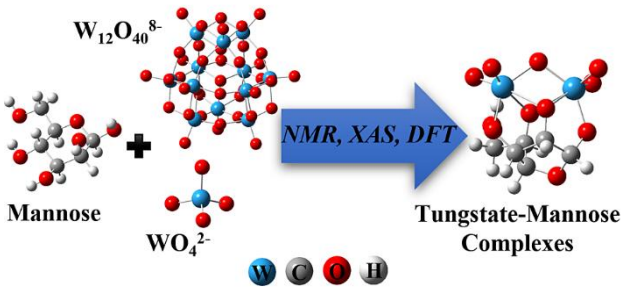

ABSTRACT : The control of metal-sugar complexes speciation in solution is crucial in an energy transition context. Herein, the formation of tungstate-mannose complexes is unraveled in aqueous solution using a multi-technique experimental and theoretical approach. ^{13}C nuclear magnetic resonance (NMR), as well as ^{13}C-^{1}H and ^{1}H-^{1}H correlation spectra, analyzed in the light of coordination induced shift methods and conformation analysis, were employed to characterize the structure of the sugar involved in the complexes. X-ray absorption near edge

structure (XANES) analysis were performed to provide relevant information about the metal electronic and coordination environment. The calculation of ^{13}C NMR chemical shifts for a series of tungstate-mannose complexes using density functional theory (DFT) is key to distinguish between several candidate structures. Furthermore, a parametric study based on several relevant parameters, namely, pH and tungstate concentration was carried out to look over the change of the nature and concentrations of the complexes. Two series of complexes were detected, in which the metallic core is either in a ditungstate or a monotungstate form. With respect to previous proposals, we identify two new species. Dinuclear complexes involve both α- and β-furanose forms chelating the metallic center in a tetradentate fashion. A hydrate form chelating a ditungstate core is also revealed. One monotungstate complex appears at high pH, in which a tetrahedral tungstate center is bound to α-mannofuranose through a monodentate site at the second deprotonated hydroxyl group. This unequalled level of knowledge opens the door to structure-reactivity relationships.

Introduction

Rapid world's population growth has led to increasing demand of energy and commodity chemicals, whose production is so far heavily reliant on fossil resources. In addition, the rising environmental concerns coupled to a depletion of conventional fossil fuels has made mandatory the exploration of non-edible alternative energy sources. Lignocellulose,[1] a natural carbon source collected from plant biomass, is a particularly abundant renewable feedstock that has drawn significant attention as a sustainable raw-material for the production of renewable energy and high added-value products including chemicals, biofuels, and advanced materials without compromising food security.[2–5] Lignocellulosic biomass is typically composed of a cellulose skeleton surrounded by hemicellulose and lignin with varying percentages depending on the origin of the plant. Cellulose and hemicellulose are polysaccharides that can be depolymerized

into various monosaccharides. Among the components of lignocellulose, upgrading the carbohydrate-containing parts (cellulose and hemicellulose) seems at first glance easier due to their chemical nature. However, despite the large body of research work dedicated to both fundamental and applied studies on the chemical reactivity of carbohydrates to produce platform chemicals,[6–8] at that date only a few industrial processes have been fully developed up to the industrial scale. The very recent pilot plant developed by Avantium for the hydrogenolysis of sugars to produce ethylene glycol is one of these rare examples.[9] The main challenges lie in the development of selective catalysts,[10] and gaining fundamental insight in the catalytic transformation of sugars will be of importance in that respect.

Metal ions are known to take part in many chemical reactions undergone by sugars.[11–18] More particularly, tungstate salts were found to be efficient catalysts for the cleavage of the carbon chain producing the proper chemical intermediates that are precursors for the synthesis of short chain polyols such as ethylene glycol, propylene glycol or glycerol.[13–17] Metal-sugar interactions are expected to occur in order to achieve these reactivities.[12,14] However, the coordination complexes of metal centers with sugars are not unambiguously identified to date.[19] Although the sugar-metal coordination chemistry has been known for a very long time, noticeably for its participation in biochemical processes, in particular calcium,[20,21] only recent studies employ DFT calculations to unravel its reactivity in carbohydrate conversion chemistry for the production of chemicals.[22–26] Sugars may be polydentate ligands of L type (through hydroxy groups)[26–28] or X type (after deprotonation)[29–31] to various metal ions. However, only few works address computationally their complexes with tungstate species, either homogeneous[29] or heterogeneous.[31]

In the present work, we aim at unraveling the structure of carbohydrate-metal complexes in the prototypical case of tungstate-mannose interaction in aqueous solution,[32] as it is the required step for the understanding of the reactivity of those complexes. Mannose can be efficiently

converted into platform molecules either in aqueous or organic medium.[33,34] For instance, by reacting with tungsten oxides, mannose is able to achieve high yields of ethylene glycol.[13] This carbohydrate belongs to the polyhydroxy aldehydes family and can exist in aqueous solution in five-membered or six-membered rings named respectively furanose and pyranose, or under its linear form, hydrated or not (***Figure S.1.*** in the **Supporting Information**).[35] This complexity makes the structural identification of metal-sugar complexes a hard task, which is the goal of the present work.

Aqueous tungstate oxyanions speciation depends on the pH and the total tungsten concentration.[36] Monooxyanions and polyoxyanions forms are encountered. Monomeric species, that are known to occur in tetrahedral geometry prevail at high pH and lower tungsten concentration, while at lower pH, polymeric species of local octahedral geometry predominate. Previous studies were devoted to the characterization of tungstate carbohydrate complexes.[32,37–39] Complexes involving W^{6+} ditungstate cores were evidenced according to multinuclear ^{183}W and ^{13}C nuclear magnetic resonance (NMR) spectroscopies. Complexes referenced as L and M were reported with D-mannose (***Figure 1***).

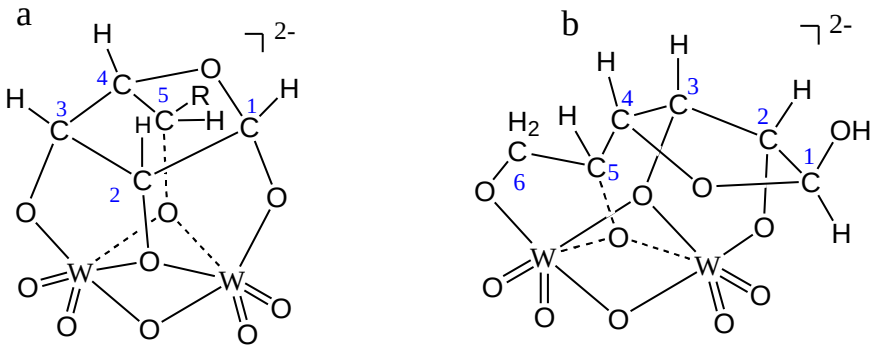

Figure 1. *Proposed structures for tungstate complexes of D-mannose. (a) L type, R= CH_2OH (b) M type. Adapted from [32,37]*

Several techniques were employed for the characterization of tungstate-carbohydrate complexes including mainly multinuclear NMR spectroscopies, circular dichroism, potentiometry and X-Ray crystallography for the few complexes that tend to crystallize.[40–43]

However, some strong missing points remain important for the structural clarification of these species, and in particular in the interplay between these species and their speciation in aqueous phase. Obtaining crystal structures is quite difficult for such species, and besides, the composition of the crystalline phase may not reflect that present in aqueous solutions, as is the case for most sugars and tungstate oxyanions species, although the latter is the most relevant to catalytic conditions. All of these complexes were identified in a limited pH range without reporting the effect of varying the metal ions concentration and the pH on the nature of theses organometallic species. Moreover, all the syntheses of these complexes were carried out in a 2:1 metal/sugar stoichiometry. Although density functional theory (DFT) computational methods have proven being powerful tools for the investigation of molecular structures and the quality of the theoretically computed ^{13}C NMR chemical shift is considered trustworthy,[44,45] to the best of our knowledge, no computational study was reported for the structural clarification of these carbohydrate complexes.

Therefore, in the present work, we show a full methodology for the characterization of tungstate-mannose aqueous mixtures using a combined spectroscopic and theoretical procedure. We combine ^{13}C NMR and X-ray absorption Near Edge Structure (XANES) spectroscopies to probe the state of the carbohydrate ligand and the metal ion, respectively, and screen various conditions for the formation of the complexes (pH, metal ion concentration and metal/mannose ratio). The calculation of ^{13}C NMR chemical shifts for a series of tungstate-mannose complexes at the DFT level of theory is key to choose between several possible candidates based on experimental observations. Thanks to this approach, we reach an unequaled level of knowledge on the structure of these complexes as a function of operating conditions. On top of the two previously proposed species (***Figure 1***) which existence is confirmed, we reveal two new dimeric and monomeric species with respect to previous proposals, that are likely to play a key role in the further transformation of sugars.

Experimental section

Preparation of tungstate-mannose complexes

The complexes were prepared in aqueous solutions at room temperature, by mixing mannose with various precursors of tungsten, namely sodium tungstate dihydrate ($Na_2WO_4 \cdot 2H_2O$) and ammonium metatungstate [$(NH_4)_6H_2W_{12}O_{40}$] (AMT). All the chemicals were commercial products of purest analytical grade (Sigma-Aldrich) and used as received. In a typical experiment, 1 mmol of the sugar and 2 mmol of the metallic precursor were dissolved at room temperature in 1 mL of D_2O (metal/sugar stoichiometry of 2:1, concentration of 1 and 2 mol L^{-1} respectively). The effect of the pH, metal/sugar ratio and initial chemical structure of the metallic salt on the relative nature and the proportions of the generated complexes at equilibrium were explored. The pH of the solutions was measured using a conventional glass electrode apparatus, and the pH was adjusted to the desired value by addition of a few drops of either HCl or NaOH solutions (concentrations of 10 and 3 mol L^{-1} respectively).

Nuclear Magnetic Resonance (NMR) spectroscopy

All NMR spectra were recorded on a Bruker Avance III spectrometer (300 MHz) equipped with a Broadband probe (BBFO) at 300 K.

1D-NMR Spectra: The applied frequencies were respectively 300.13 and 75.47 MHz for ^{1}H and ^{13}C nuclei. ^{1}H NMR chemical shifts were referenced using residual solvent peak for proton resonance of deuterium oxide (4.79 ppm). Proton spectra were obtained with an acquisition time of 3.4 s, a pulse duration of 14 µs with 6.7 W power pulse force and a sweeping range of 4807.7Hz. The relaxation delay was of 2 s. 1D proton decoupled ^{13}C spectra were recorded with the following parameters: acquisition time of 1.66 s, pulse duration of 9 µs with 38.8 W power pulse force, relaxation delay of 2 s and a sweeping range of 19736.8 Hz. In both experiments, the number of scans was adjusted according to the sample.

2-D NMR spectra: The 2D ^{1}H-^{1}H correlation spectroscopy (COSY) spectra were acquired using the following acquisition parameters: 1 scan, 16 dummy scans, a 1.3 s relaxation delay, a spectral width of 3.7 ppm, a transmitter offset of 5 ppm, and an acquired spectral size of 512 data points in the F1 dimension and of 2048 data points in the F2 dimension. The 2D ^{1}H-^{13}C heteronuclear single quantum correlation (HSQC) spectra were obtained with the following acquisition parameters: 2 scans, 16 dummy scans, a 1.5 s relaxation delay, a spectral width of 3.7 ppm (F2) and 180 ppm (F1), a transmitter offset of 5 ppm (F2) and 90 ppm (F1), a mean coupling constant $^{1}J_{C-H}$ for the intensive nuclei enhanced by polarization transfer (INEPT) to 145 Hz, an acquired spectral size of 256 data points in the F1 dimension and 1024 data points in the F2 dimension.

X-ray absorption spectroscopy (XAS)

XAS spectra at the W L_3-edge (10207 eV) were acquired at the European Synchrotron Radiation Facility (Grenoble, France) at the CRG-FAME BM30 beamline (French Absorption spectroscopy beamline in Material and Environmental science). Storage ring was operated at 150 mA with refill every hour. Spectra were recorded at the W L_3-edge in transmission mode using Si diodes collecting photons scattered by a kapton foil. Energy of the monochromatic beam was tuned using a Si(220) liquid-nitrogen cooled double-crystal monochromator surrounded by two Rh-covered mirrors for harmonics rejection.[46] Second crystal of the monochromator was dynamically bent in order to focus the beam on the horizontal direction. First mirror curvature was adjusted in order to collimate the beam on the vertical direction, and so to optimize the energy resolution and the photons flux on the sample, while second mirror was bent in order to focus the beam on the vertical direction. Thanks to these elements, the beam spot on the sample was 200 × 100 μm² (HxV, full width half maximum values). Energy calibration was ensured for each scan by measuring the XAS signal of a W metallic foil in double transmission, simultaneously to the studied solutions. Energies was then set to 10207 eV

at the maximum of the W foil spectrum first derivative. Measurements were performed at 10 K using a liquid helium cryostat to preserve solutions from any radiation damages. All processing of the spectra was carried out using the Demeter software suite.[47]

Computational methods

DFT calculations were performed by employing the B3LYP hybrid exchange-correlation functional[48,49] with the Gaussian 09 software suite.[50] Geometry optimizations were done using the def2-tzvp basis set for W atoms[51,52] and tzvp basis sets for C, H and O atoms.[51–54] All the calculations were carried out using an implicit solvent model (water) in the frame of the SMD solvation model.[55] SCF calculations were performed with a 0.418 $kJ.mol^{-1}$ convergence criterion on the total energy. For geometry optimizations we used a convergence criterion of the force on all atoms of $3\ 10^{-4}$ Ha/Bohr. In the following manuscript we only report structural and spectroscopic features of the complexes and not the energies as the latter were found to be strongly dependent on the protonation state of the complexes and other calculation parameters such as the applied solvent model. The energetic data for the complexes reported in the manuscript are given in **Supporting Information** (***Table S1*** *and* ***S2***). To compare with experimental NMR measurements, the chemical shielding of the optimized structures has been calculated at the same level of theory using the Gauge-Independent Atomic Orbital (GIAO) method[56,57] and referenced to calculated chemical shielding of DMSO for carbon and hydrogen atoms in order to determine ^{1}H and ^{13}C chemical shifts. DFT results were then compared to the NMR measurements of our own experiments to find out the models that fit the best with the experimental data. In order to benchmark the accuracy of the calculation method, ^{13}C chemical shifts of a series of three well-known sugars (glucose, mannose, and fructose) in their different tautomeric forms were calculated. The corresponding parity plots are given in the **Supporting Information** (***Figure S.2.***). A mean relative error of 1.4% is obtained in the range of 60-

120 ppm for carbon, showing the reliability of the DFT in the prediction of NMR chemical shifts.

Results and discussion

NMR spectroscopy

The formation of tungstate-mannose complexes at neutral pH (7.5) was experimentally detected by the apparition of several new sets of six peaks in the ^{13}C NMR spectrum compared to that of free mannose. ***Figure 2,a*** illustrates the proton-decoupled ^{13}C NMR spectrum of a D-mannose-sodium tungstate solution in deuterium oxide (D_2O) at pH 7.5. The complexes were then characterized after full assignment of the carbon signals and protons bound to them by means of two-dimensional ^{1}H-^{13}C heteronuclear (HSQC) and ^{1}H homonuclear (COSY) NMR experiments (***Figures 2,b,c***). Three different species were detected and denoted complexes A, B, and C. When sodium tungstate was mixed with mannose without adding any extra base or acid to the aqueous medium, a solution of approximatively pH 9 was obtained. In this case, a new set of six peaks appeared in the ^{13}C NMR spectrum recorded for this solution. The existence of a complex, further referred to as complex D, was verified by the increase in intensity of the new peaks in the carbon spectrum of the solution obtained at pH 11 (***Figure 2,d***).

Besides, adjusting the pH of AMT-mannose aqueous solutions to around 7 and 11 leads to the formation of the same complex. Its existence is thus essentially related to the speciation of tungstate ions (that depends on the pH) in the aqueous solution rather than to the nature of the metallic precursor.

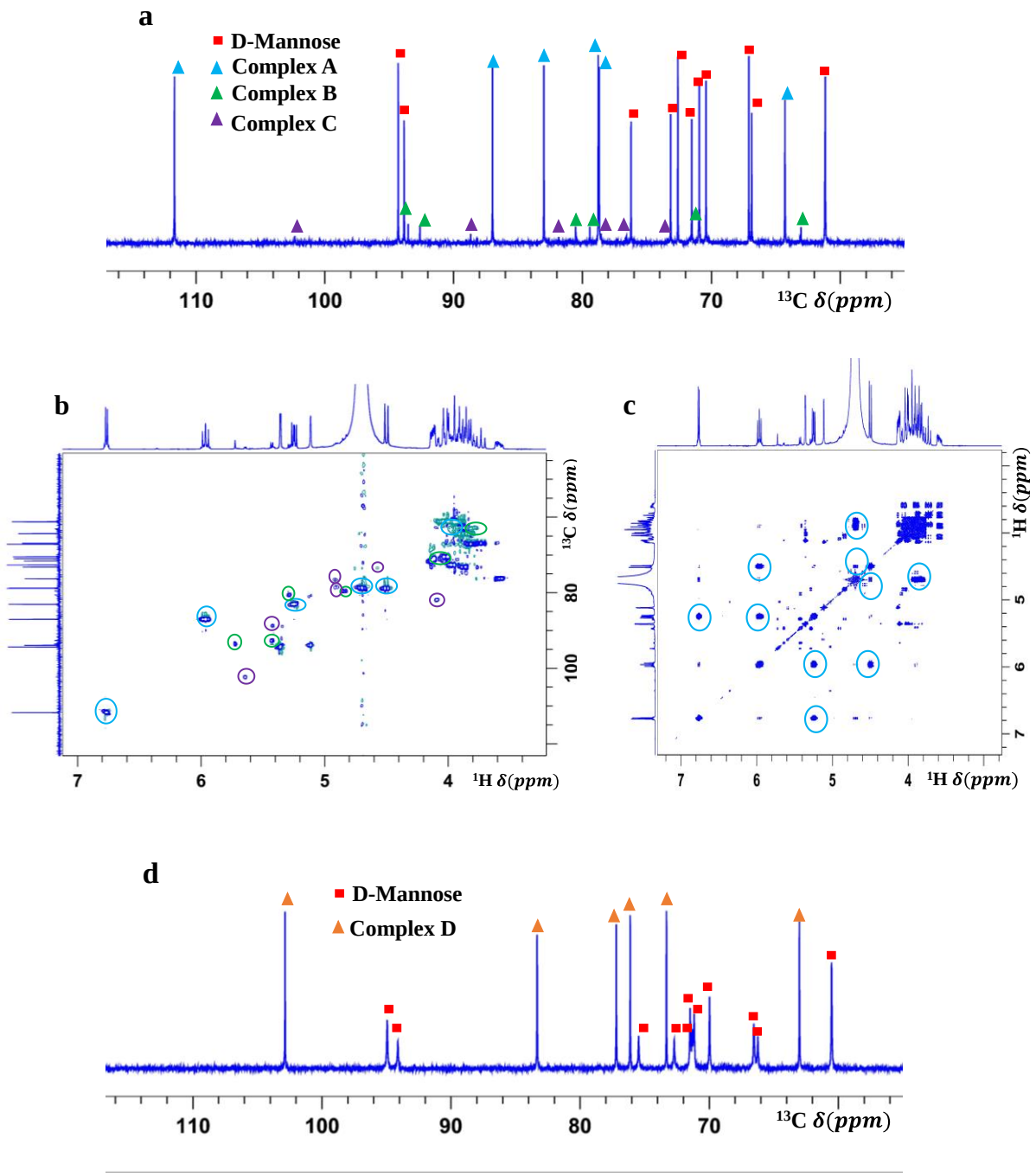

Figure 2 : *(a) Proton decoupled ^{13}C NMR spectrum, (b) heteronuclear single quantum correlation ^{1}H-^{13}C NMR spectrum (row: ^{1}H, column: ^{13}C), (c) ^{1}H homonuclear NMR correlation spectrum of the solution of sodium tungstate with D-mannose at pH 7.2, sugar and W concentrations of 1 and 2 mol L^{-1} respectively. The circles depicted in the 2D spectra correspond to the correlation between the carbon atoms and the proton(s) attached to them in addition to the correlation between vicinal protons respectively in the HSQC and the COSY spectra, (d) Proton decoupled ^{13}C NMR spectrum of sodium tungstate-D-mannose aqueous solution at pH 11, sugar and W concentrations of 1 and 2 mol L^{-1}.*

Previous works described two tungstate complexes with D-mannose denoted types L and M, the former being the major product and the latter the minor product. Complex L (***Figure 1,a***) is characterized by mannose in its β-furanose form chelating a ditungstate ion core at the HO1,2,3,5 site, while complex M involves the α-furanose form of mannose chelating a ditungstate core as well, though by the HO2,3,5,6 site[58,59] (***Figure 1,b***). ***Table 1*** illustrates the chemical shifts recorded in the carbon spectra of the different species.

Table 1: *^{13}C NMR chemical shifts (in ppm) of tungstate-D-mannose complexes.*

Carbon atom	**C1**	**C2**	**C3**	**C4**	**C5**	**C6**
Complex L[60]	112.7	84.0	88.0	79.7	79.7	65.2
Complex M[60]	103.6	89.7	79.5	77.5	82.6	74.3
Complex A	111.7	83.2	87.1	78.8	78.7	64.3
Complex B	93.6	92.6	80.5	79.5	71.0	63.1
Complex C	102.6	88.6	78.5	76.6	81.9	73.4
Complex D	103.5	83.7	76.7	78.1	73.5	63.6

The carbon chemical shifts displayed for Complexes A and C in our study are in line with that of complexes L and M of previous studies, respectively (***Table 1***). However, no chemical structures were proposed for complexes B and D.

Possible ligands for each complex were deduced from the deshielding of the carbon atoms of all the possible oxygen donor adducts by a Coordination Induced Shift (CIS) value, which displays a characteristic pattern for each type of complex. The CIS value is calculated as the difference between the chemical shift of the same carbon atom in the complexed and the free form of the sugar according to ***Equation 1***. The literature did not set a threshold for the downfield shift exhibited by the coordinated carbon atoms. However, a minimum deshielding of 5 ppm was perceived while discussing tungsten and molybdenum complexes of carbohydrates.[61,62]

$$CIS = \delta(complexed\ sugar) - \delta(free\ sugar) \qquad \textbf{Equation 1}$$

Since naturally, sugars occur in six different forms including five tautomers (four cyclic and one acyclic) and an acyclic hydrate species, the CIS value pattern was calculated with reference to all experimental chemical shift values of the six free forms of D-mannose in order to determine the possible ligand. Herein, the acyclic aldehyde was discarded since no signal was acquired at around 200 ppm which is a fingerprint of the existence of a carbonyl group. The CIS values are respectively shown in ***Tables S3-S6*** in the **Supporting Information**.

For the assignment of complex A (***Table S3,*** **Supporting Information**) we observed by assuming α- and β- pyranose as ligands, four high coordination induced chemical shifts values at the first four carbon atoms of the two anomers, indicating the possibility of the existence of four chelation sites through their deprotonated hydroxyl groups. However, by considering the stereochemistry of the molecules (***Figure S.1.,*** **Supporting Information**) we found the chelation inconceivable since the hydroxyl groups are *trans*-oriented. The CIS patterns calculated by assuming α- and β-furanose as ligands, indicates that C1,2,3,5 are deshielded, subsequently O1,2,3,5 (numbered similarly as the carbon atom connected to O) should be the chelation sites. However, this connection is only feasible for β-furanose in which HO1,2,3 are *cis*-oriented with each other with respect to the ring while for α-furanose the anomeric hydroxyl group is *trans*-oriented. Moreover, by supposing the acyclic hydrate mannose as a ligand, four high CIS values appear at the first four vicinal carbon atoms C1,2,3,4.

As for complex B (***Table S4,*** **Supporting Information**), three high induced chemical shifts are obtained at the O2,3,4 site by proposing α- and β-mannopyranose as ligands. However, the hydroxyl group of the fourth carbon atom is *trans*-oriented to O2,3 discarding the possibility of forming an adduct for complex B. α- and β-furanose constitute proper candidates by displaying two high coordination induced shifts at their second and third carbon atoms raising the possibility of the presence of a bidentate complex. In addition, hydrated mannose displays 4 high induced chemical shift at O2,3,5,6 site, indicating the possible presence of a

tetradentate chelated species. By considering the hydrated mannose as a ligand, three downfield shifts higher than 5 ppm were detected at O2,3,4 possible coordination site. However, according to the DFT data that are discussed below, hydrated mannose probably chelates the metal ion through four deprotonated oxygen atoms displaying only a small shift for the first carbon atom.

Regarding complex C, by considering the pyranose forms, all the carbon atoms are deshielded, which eliminates their possibility to be ligands since their corresponding hydroxyl groups are *trans* oriented. Under the hypothesis of an α-furanose form, four high induced chemicals shifts are obtained at C2,3,5,6 positions indicating the possibility of the presence of a tetradentate chelation mode (***Table S5,*** **Supporting Information**). With β-furanose, five high induced chemical shifts at the C1,2,3,5,6 positions suggest the possibility of chelation through O1,2,3,5,6 sites. Moreover, by supposing hydrated mannose as a ligand, five high CIS values were obtained at the C1,2,3,5,6 positions, thus revealing one more additional complexation possibility.

For complex D (***Table S6,*** **Supporting Information**), following a similar reasoning, we find that if the sugar is complexed in its α-pyranose form, four high CIS values at C1,2,3,4 site are obtained, though this includes hydroxyl groups that are *trans*-oriented which eliminates its possibility to be considered as the proper ligand. Similarly in the case of β-pyranose, three high CIS values exist at the C1,2,4 positions, however, the corresponding hydroxyl groups are *trans* oriented, which discards this possibility. By considering α-furanose as a ligand, a single downfield shift (higher than 5 ppm) is detected at the second carbon atom C2, prompting the presence of a possible monodentate complexation. With the β-furanose hypothesis, three deshielded carbon atoms were detected through the tridentate C1,2,3 site. Considering the hydrate form, four high chemical shifts manifested at the C1,2,3,4 site, thus proposing the presence of a tetradentate chelation site. Thus, two ligand possibilities remain concerning the

form of mannose in the A complex (β-furanose and acyclic hydrate), and 3 ligands forms remain possible for B, C, and D complexes, based on CIS and conformation considerations.

pH and tungsten concentration effect

The tungstate concentration and the pH were changed systematically. The percentage of each complex was estimated from the relative areas of the carbon signals considering for each the signal of the anomeric carbon. ***Figure 3,a*** shows the effect of the metal ion concentration on the nature of the formed complexes. The study was carried out at pH around 7.5 and a constant sugar concentration of 1 mol L^{-1}. With decreasing metal ion concentration, the concentrations of the complexes decrease without a change in the nature of the species (details about the estimated amounts of complexes as well as the quantity of the metal ion involved in the complexation are provided in ***Table S7*** in the **Supporting Information**). The relative amount of each complex is mostly independent of the concentration of the metal ion, which suggests a similar nuclearity of the metal ions in the different complexes. This conclusion is only valid for complexes A, B and C since the study was carried out at pH around 7.5 at which species D was not observed.

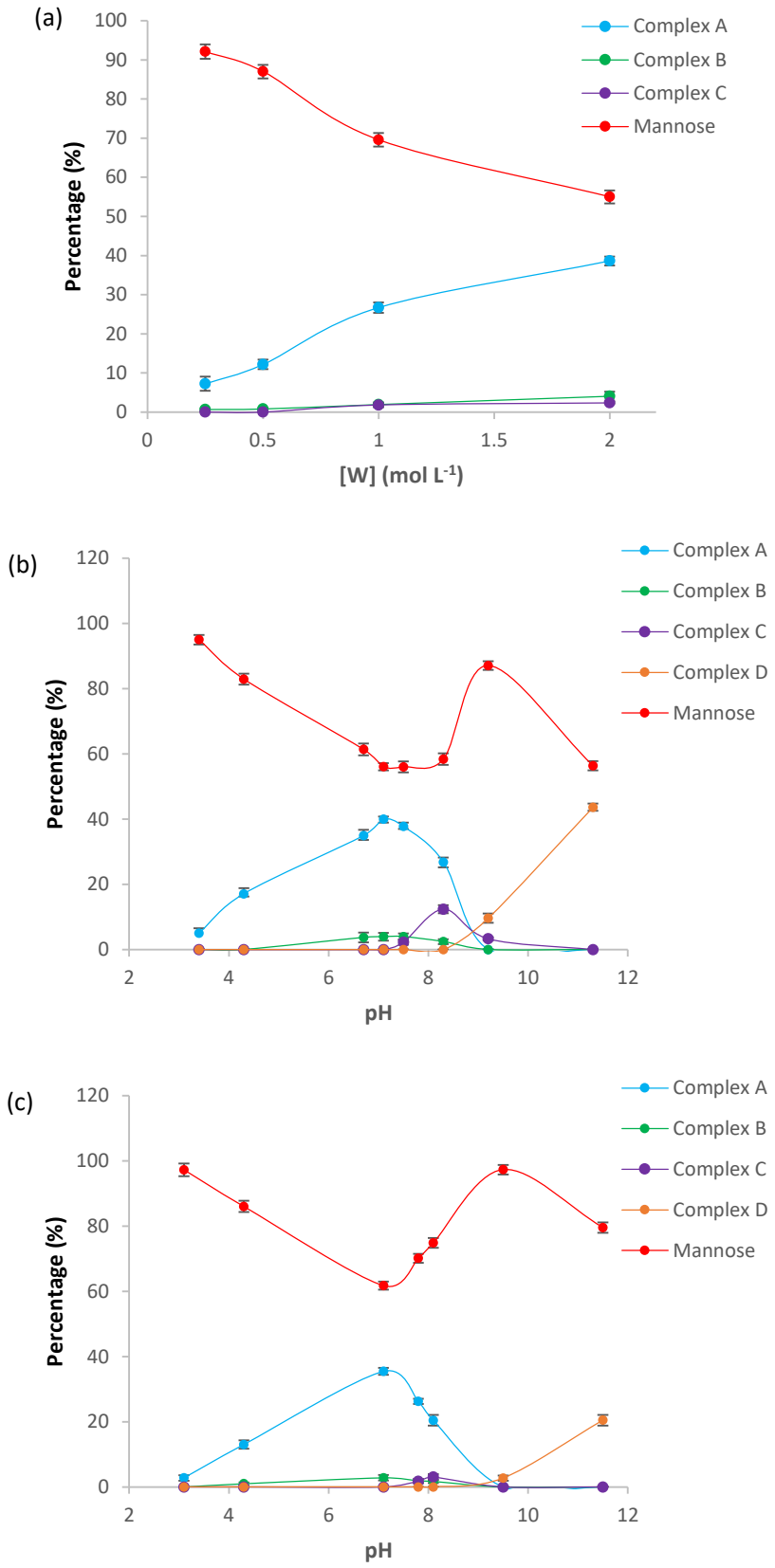

Figure 3. *Concentration of Complexes A, B, C and D in a series of sodium tungstate and mannose solutions as function of* ***a)*** *tungsten concentration (mol L^{-1}) (pH 7.5 and mannose concentration of 1 mol L^{-1}) and pH,* ***b)*** *(tungsten and mannose concentrations of 2 and 1 mol L^{-1} respectively) and* ***c)*** *(tungsten and mannose concentrations of 1 and 1 mol L^{-1} respectively).*

The evolution of the proportion of tungstate complexes as function of pH in a series of D-mannose and sodium tungstate aqueous solutions was also investigated and is illustrated in ***Figure 3,b,c***. Generally, the maximum amount of species A and B was simultaneously observed at pH around 7 in both tungstate solutions independently of the tungsten/mannose ration. Species A remains the dominant species while B is the minor species over the pH range 2-8. Moreover, the amount of complex A slightly decreases by reducing tungsten concentration indicating that the amount of complexed tungsten ions increases while lowering the concentration of tungsten (see ***Tables S8 and S9*** in the **Supporting Information**). Species C and D display a different behavior, with complex C having a maximum concentration around pH 8-8.5 in the highly concentrated tungstate solution ([W] = 2 mol L^{-1}), though remaining a minor species. However, with decreasing tungsten concentration ([W] = 1 mol L^{-1}) the amount of the current species does not exceed 3%. Complex D appears only above pH 8 and becomes the dominant species at higher pH values, reaching around 44% and 20% of abundance at pH 11 with respectively 2/1 and 1/1 of tungsten/mannose ratio. The observation of a pH-dependent speciation of the complexes is of a high importance for the involvement of the complexes in catalysis.

The results presented herein allow for an important observation regarding the nuclearity of the species. At the maximum amount of species A (the major species in neutral solutions) and B, the proportion of complexed sugar is of about 42 %. Given that the molar ratio W/sugar equals 2 (for the data reported on Figure 3-b), considering the *maximal* hypothesis under which 100 % of W atoms are involved in the formation of these complexes (ie considering that their formation reaction are total) yields the *maximal* nuclearity of this complexes of 4.7. The same reasoning done on the data shown on Figure 3c (ratio W/sugar of 1 and maximum amount of complexed sugar of 32 % at pH 7) yields a maximum nuclearity of 3.1 for complex A. Clearly,

the complexes detected herein have a lower nuclearity than that of the most abundant W oxyanions in such concentration and pH conditions ($W_{12}O_{40}^{8-}$ according to the Medusa simulations presented in ***Figure S3*** in the ***Supporting Information***). This is in line with early proposals referring to binuclear species for sugars-tungstates or molybdates complexes, and further demonstrates that the equilibria of tungsten oxyanions in aqueous solution are strongly shifted by the presence of sugars.

XAS

Tungstate-sugar mixtures have been analyzed by X-ray Absorption Spectroscopy at the W L_3-edge, a technique widely used for investigation of the environment of metals for such kind of compounds.[58,59] First, we recorded the spectra of tungstate aqueous solutions of both precursors used in this study, sodium tungstate and ammonium metatungstate (AMT), in order to reference the edge energy of W^{6+} since they are fully oxidized metallic salts and to distinguish the spectroscopic features of tetrahedral and octahedral species, respectively. ***Figure 4*** shows the W L_3-edge XANES spectra of sodium tungstate, AMT and mannose-tungstate aqueous solutions at different pH values recorded in transmittance mode, in addition to the first derivatives of the spectra.

The white line appearing in the L_3-edge XANES of tungsten is mainly attributed to electronic transitions from $2p_{2/3}$ orbitals to vacant 5d orbitals.[59] According to ***Figure 4,a***, a relationship between the structure of the WO_x unit and the shape of the white line exist. Sodium tungstate provides monotungstate oxyanions in aqueous solution, (pH around 9) occurring in tetrahedral geometry while ammonium metatungstate (pH around 4) provides polymeric clusters in which the WO_x moieties have six-fold coordination environment, thus occurring in octahedral geometry.[36,59] As shown on ***Figure 4,a,*** the aqueous solution of ammonium metatungstate shows a broad peak with a splitted top with an energy gap of around 3.6 eV (second derivative in ***Figure S4*** in the **Supporting Information**) between the peaks which is

a characteristic of distorted octahedral structures.[59] This splitting can also be observed on the first derivative plot (***Figure 4,b***) by the appearance of a second maximum. Sodium tungstate (Na_2WO_4) displays one sharp asymmetrical peak due to the negligible splitting of the 5d state of the tetrahedral tungsten center. These findings agree with the literature, which tends to show that the more centrosymmetric the metallic center is, the greater is the energy gap between the splitted peaks. Indeed, tungsten centers in Cr_2WO_6, which have a quasi-perfect octahedral geometry, display an energy gap of 5.6 eV while the distorted tungsten centers of ammonium metatungstate provide an energy gap of 3.8 eV,[59] which is similar to the value obtained in our current experiment. Another characteristic of tetrahedral coordinated sites that has not been previously discussed in other articles is the presence of a bump at around 15 eV beyond the edge energy such as in the spectrum of sodium tungstate (Na_2WO_4) (***Figure 4,a***).

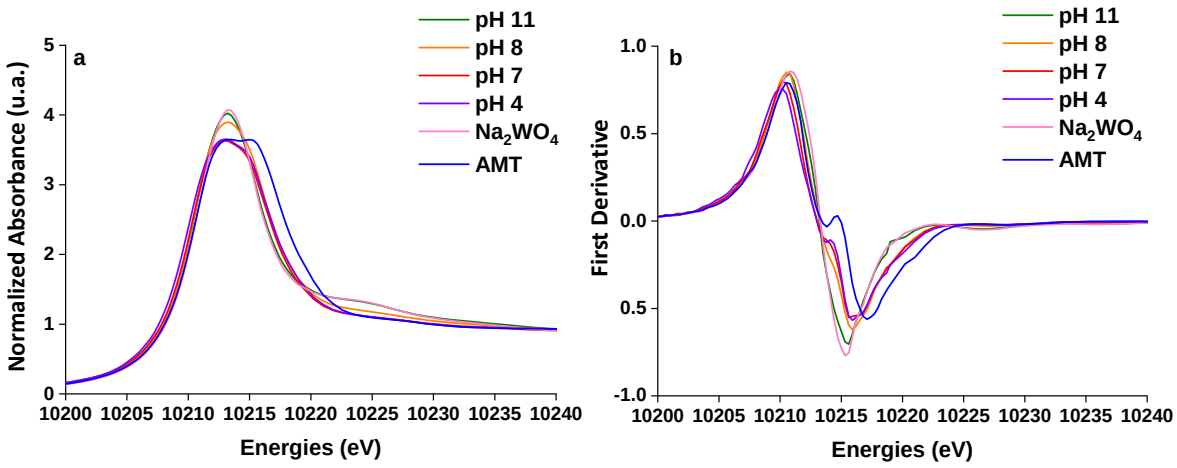

Figure 4. *(a) W L_3-edge XANES normalized spectra, (b) first derivative of (a) of reference tungstate precursors in aqueous solution: ammonium metatungstate AMT and sodium tungstate Na_2WO_4 as well as tungstate-mannose aqueous solution at different pH values. [W] = 0.1 mol.L^{-1}, [Mannose] = 0.1 mol.L^{-1}.* the experiments were conducted at such low tungsten concentration to prevent fluorescence phenomena. The effect of changing tungsten and mannose concentrations while conserving the same W/sugar ratio was almost ineffectual for the amount of complexed tungsten (See* ***Table S10*** *in the* ***Supporting Information****).*

The edge energy is quantified by evaluating the maximum of the first derivative of the signal. The values detected for both precursors in aqueous solution are of 10210.8 eV (***Figure***

4,b). The edge energy as determined by the maximum in the first derivative spectra of crystalline sodium tungstate and solid ammonium metatungstate are respectively of 10210.6 and 10209.9 eV. All the species correspond to W^{6+} oxidation state. Concerning tungstate-mannose aqueous mixtures (***Figure 4,a***) at pH 11 and 8, the edge energy is around 10210.6 eV while at pH 7 and 4, the edge energies are respectively, 10210.2 and 10210.0 eV indicating that tungsten centers in the complexes are consistent with W^{6+} oxidation state.

At pH 11 (***Figure 4,a***), the observed XANES spectrum is very similar to that of sodium tungstate aqueous solution, indicating that tungstate species of tetrahedral geometry are present in this pH range. A significant amount of complex D exists at such high pH values, though, and since it contains a minimum of one tungsten atom per sugar molecule, the amount of complexed tungsten is around 20% (see ***Table S10*** in the **Supporting Information**). The observation of a spectrum very similar to that of the tetrahedral reference Na_2WO_4 is indicative of a similar coordination environment, hence that complex D involves a tetrahedral W center. As the pH of the aqueous solution decreases to 8, 7 and 4, at which complex D does not exist anymore, being replaced by complexes A, B and C, the white line broadens while showing a splitting marked by the presence of a second maximum in the first derivative (***Figure 4,b***), an evidence of the formation of octahedral structures. Moreover, the disappearance of the bump at 15 eV after the edge energy with the decreasing of pH confirms that a conversion from tetrahedral sites to octahedral sites occurs. However, at pH 8, the bump is slightly manifesting at 15 eV beyond the edge energy, pointing to the contribution of tetrahedral tungsten sites. In fact, in such conditions (tungsten concentration of 0.1 mol L^{-1}, pH 8), the free tungstate exists only in monomeric form (***Figure S3*** in the **Supporting Information**), the addition of the sugar leads to a partial complexation of the metal ions indicating that the complexed metallic ions are of octahedral geometry while free tungstate ions remained in their monomeric form. The splitting of the white line of this sample is 3.0 eV, *vs.* 3.6 for AMT, revealing that the octahedral species

formed are of more distorted octahedral geometry. Nevertheless, the spectra at pH 7 and 4 (showing no additional bump at 15 eV beyond the edge energy) are clearly distinct from the spectra of the precursor, for instance the splitting of the white line is only of 3.3 eV, *vs* 3.6 eV for AMT, indicating that a distinct yet also octahedral species coexist. Thus, these results are indicative that the tungsten centers of complexes A, B and C are rather in distorted octahedral symmetries. Note that these observations are made at pH 7 and 4 despite the presence of uncomplexed AMT (around 30 % assuming the formation of a dinuclear complexes) that nevertheless contribute to the XANES signal.

Consequently, mannose generates complexes when it is mixed with tungstate precursors in aqueous solution. These complexes comprise W^{6+} centers as verified with reference to the edge energy of the fully oxidized tungstate salts (Na_2WO_4 and AMT), although we cannot exclude that the picture could be different under reductive atmosphere such as the one used in some catalysis experiments. Among all of the formed species, one complex, denoted D, corresponds to a mononuclear tetrahedral metallic center. The three other species revealed by NMR at lower pH (A, B, C) contain an oligomeric tungsten core in octahedral geometry. The attribution to the coordination sites is possible by analyzing the increase of the NMR chemical shift of the carbon atom, however several possible structures remain possible after analyzing the NMR data along with the conformation considerations. Hence, in order to clarify the molecular structures of the complexes, we performed a computational analysis at the DFT level.

Computational study

In this section we provide a screening of potential interactions between tungstate oxyanions and D-mannose in aqueous solution at the density functional theory level. In line with the experimental findings reported above, all the models feature W^{6+} species only, as no evidence for reduction could be provided by XAS. We then examine various models featuring mannose in interaction with mono- and binuclear metallic cores, as well as with a model of the AMT

anion. Binuclear species were selected for the following reasons: (i) this matches earlier proposals from the literature (ii) this also matches the observation that complex A has a nuclearity of at most 3 (iii) they can be considered as a model for a coordination site on a larger oligomer ; attempts to optimize the coordination of mannose to a $W_{12}O_{40}^{8-}$ model on a trinuclear coordination site resulted systematically in a decoordination from the third nucleus and evolved towards a coordination to a binuclear site (see below).

Considering the tetrahedral geometry of monotungstate oxyanions (WO_4^{2-}), complexes of monodentate, bidentate and tridentate coordination were chosen in the current study for the mononuclear complexes (***Figure 5,a,b,c***). For the binuclear species, and in line with the experimental results obtained, we explored mainly the formation of dimeric tetradentate species (***Figure 5,d***), as well as pentadentate chelation modes (***Figure 5,e***) in a 6-fold coordinated metallic site. Inorganic tungsten species in which the metallic center occurs as an octahedron are only found in polymeric forms in aqueous solution (typically with nuclearities of 6 to 12 as in $W_{12}O_{40}^{8-}$, see ***Figure S5*** in the **Supporting Information**). We decided to study metatungstate ion as a model of sugar complexes with higher nuclearity (***Figure 5,f***). We examined several geometries of the sugar in which the ligands have a similar configuration (*ie* with the same chelation sites) as in the dimeric species for which the calculated chemical shifts match the most with the experiments.

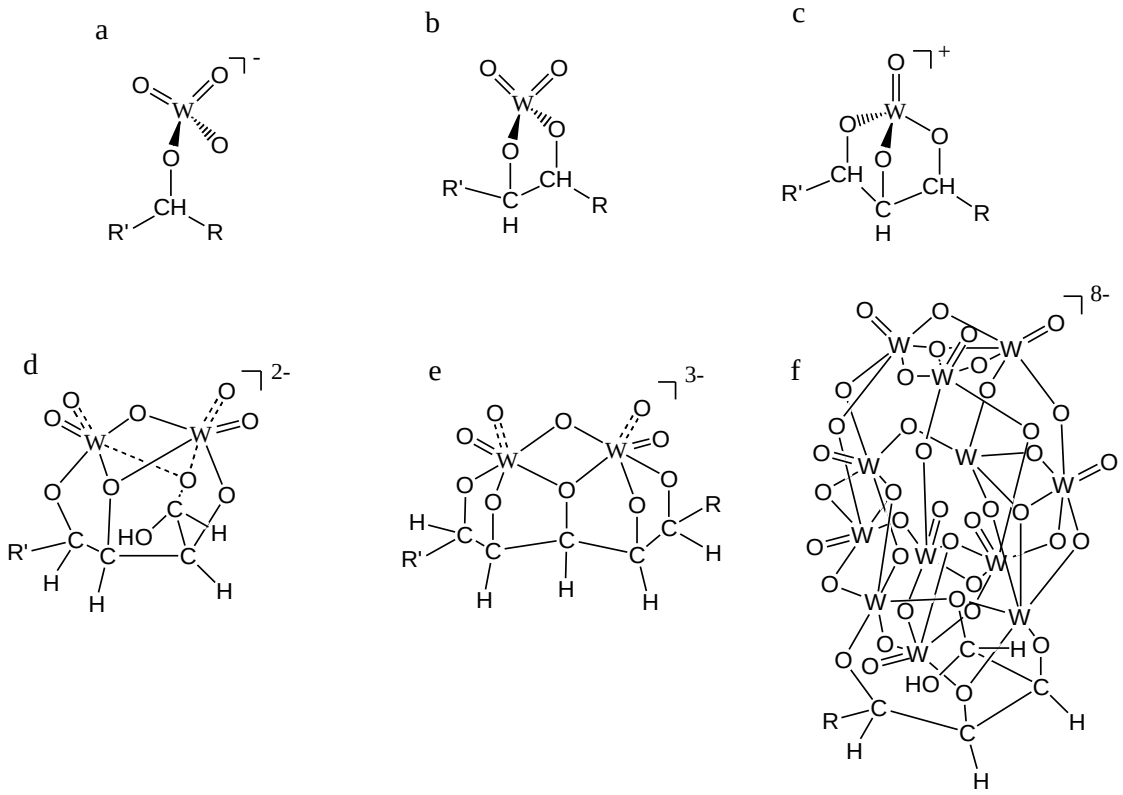

Figure 5. *Geometry of mononuclear (a) monodentate, (b) bidentate, (c) tridentate, dinuclear (d) tetradentate, (e) pentadentate and (f) polynuclear pentadentate tungstate complexes, chosen as starting points for DFT calculations. All models feature* W^{6+} *cores.*

The coordination modes were chosen according to the most relevant calculated CIS pattern for each complex as detailed above. The corresponding models are shown in ***Figures S6-S9*** in the **Supporting Information.** The identification of the complex was then done by comparing the experimental ^{13}C NMR chemical shifts to the computed values of the complexes modelled. ***Table 3*** gives the experimental ^{13}C NMR chemical shifts of complexes A, B, C and D and the theoretically computed chemical shifts values of their corresponding models. To prevent the total dissociation of the metatungstate ion in the complex, the geometries were optimized without adding a solvent model while the chemical shifts were always computed in the presence of a solvent. The effect of optimizing the molecules in a gas phase instead of using a solvent model on the computed chemical shifts was verified for the dimeric complexes presenting the best matching chemical shifts with the experiments. It has been found that the effect is negligible (see ***Table 3)***.

Table 2. Experimental ^{13}C NMR chemical shifts of complexes A, B, C and D in addition to the calculated ^{13}C NMR chemical shifts of the possible models of complexes suggested according to the experimental CIS values calculated and depicted in Tables S3-S6. in the Supporting Information.[a]

Carbon atom	Complex type	C1	C2	C3	C4	C5	C6
Complex A		***111.7***	***83.2***	***87.1***	***78.8***	***78.7***	***64.3***
Complex 1	d	*111.2**	*82.0**	*89.1**	*80.2*	*77.1**	*62.9*
$\Delta\delta_{exp,th}$		**+0.5**	**+1.2**	**-2.0**	**-1.4**	**+1.6**	**+1.4**
Complex 1 (gas phase)	d	*111.2**	*81.7**	*86.9**	*80.2*	*75.9**	*62.0*
$\Delta\delta_{exp,th}$		**+0.5**	**+1.5**	**+0.2**	**-1.4**	**+2.8**	**+2.3**
Complex 2	d	*106.8**	*86.8**	*74.0**	*76.3*	*79.7**	*64.7*
$\Delta\delta_{exp,th}$		**+4.9**	**-3.6**	**+13.1**	**+2.5**	**-1.0**	**-0.4**
Complex 3	d	*97.2**	*93.1**	*82.3**	*78.2**	*72.6*	*65.2*
$\Delta\delta_{exp,th}$		**+14.5**	**-9.9**	**+4.8**	**+0.6**	**+6.1**	**-0.9**
Complex 4	d	*101.6**	*79.0**	*75.5**	*84.5**	*76.5*	*65.2*
$\Delta\delta_{exp,th}$		**+10.1**	**+4.2**	**+11.6**	**-5.7**	**+2.2**	**-0.9**
Complex 13 (gas phase)	f	*111.7**	*83.1**	*82.9**	*79.9*	*81.1**	*63.1*
$\Delta\delta_{exp,th}$		**0.0**	**+0.1**	**+4.2**	**-1.1**	**-2.4**	**+1.2**
Complex B		***93.6***	***92.6***	***80.5***	***79.5***	***71.0***	***63.1***
Complex 3	d	*97.2**	*93.1**	*82.3**	*78.2**	*72.6*	*65.2*
$\Delta\delta_{exp,th}$		**-3.6**	**-0.5**	**-1.8**	**+1.3**	**-1.6**	**-2.1**
Complex 3 (gas phase)	d	*96.3**	*90.6**	*79.7**	*76.8**	*74.1*	*66.7*
$\Delta\delta_{exp,th}$		**-2.7**	**+2.0**	**-0.8**	**+2.7**	**-3.1**	**-3.6**
Complex 4	d	*101.6**	*79.0**	*75.5**	*84.5**	*76.5*	*65.2*
$\Delta\delta_{exp,th}$		**-8.0**	**+13.6**	**+5.0**	**-5.0**	**-5.5**	**-2.1**
Complex 5	b	*105.8*	*107.0**	*102.5**	*81.8*	*69.2*	*65.5*
$\Delta\delta_{exp,th}$		**-12.2**	**-14.4**	**-22.0**	**-2.3**	**+1.8**	**-2.4**
Complex 6	b	*97.9*	*96.3**	*95.3**	*82.1*	*70.9*	*65.9*
$\Delta\delta_{exp,th}$		**4.3**	**3.7**	**14.8**	**2.6**	**0.1**	**2.8**
Complex 14 (gas phase)	f	*98.4**	*86.5**	*90.7**	*79.8**	*71.9*	*65.3*
$\Delta\delta_{exp,th}$		**-4.8**	**+6.1**	**-10.2**	**-0.3**	**-0.9**	**-2.2**
Complex C		***102.6***	***88.6***	***78.5***	***76.6***	***81.9***	***73.4***
Complex 7	d	*107.4*	*92.2**	*83.6**	*81.7*	*86.2**	*78.0**
$\Delta\delta_{exp,th}$		**-4.8**	**-3.6**	**-5.1**	**-5.1**	**-4.3**	**-4.6**
Complex 7 (gas phase)	d	*106.3*	*91.5**	*83.0**	*80.6*	*85.8**	*74.9**
$\Delta\delta_{exp,th}$		**-3.7**	**-2.9**	**-4.5**	**-4.0**	**-3.9**	**-1.5**
Complex 8	d	*102.8*	*84.2**	*87.1**	*83.2*	*78.4**	*69.8**
$\Delta\delta_{exp,th}$		**-0.2**	**+4.4**	**-8.6**	**-6.6**	**+3.5**	**+3.6**
Complex 9	e	*104.7*	*87.2*	*76.6*	*83.4*	*81.2*	*70.7*
$\Delta\delta_{exp,th}$		**-2.1**	**+1.4**	**+1.9**	**-6.8**	**+0.7**	**+2.7**
Complex 10	e	*104.5*	*89.4*	*78.8*	*87.5*	*83.5*	*70.4*
$\Delta\delta_{exp,th}$		**-1.9**	**-0.8**	**-0.3**	**-10.9**	**-1.6**	**+3.0**
Complex 15 (gas phase)	f	*104.2*	*82.1**	*87.3**	*75.8*	*88.1**	*69.8**
$\Delta\delta_{exp,th}$		**-1.6**	**+6.5**	**-8.8**	**+0.8**	**-6.2**	**+3.6**
Complex D		***103.5***	***83.7***	***76.7***	***78.1***	***73.5***	***63.6***
Complex 3	d	*97.2**	*93.1**	*82.3**	*78.2**	*72.6*	*65.2*
$\Delta\delta_{exp,th}$		**+6.3**	**-9.4**	**-5.6**	**-0.1**	**+0.9**	**-1.6**
Complex 4	d	*101.6**	*79.0**	*75.5**	*84.5**	*76.5*	*65.2*
$\Delta\delta_{exp,th}$		**+2.0**	**+4.7**	**+1.2**	**-6.4**	**-3.0**	**-1.6**
Complex 11	a	*103.5*	*81.3**	*74.2*	*76.7*	*73.2*	*65.2*
$\Delta\delta_{exp,th}$		**0.0**	**+2.4**	**+2.5**	**+1.4**	**+0.3**	**-1.6**
Complex 12	c	*118.7**	*98.0**	*103.3**	*91.8*	*70.2*	*65.0*
$\Delta\delta_{exp,th}$		**-15.2**	**-14.3**	**-26.6**	**-13.7**	**+3.3**	**-1.4**

[a]The structures of the proposed complexes are illustrated in Figures S4-S7 in the Supporting Information. *Asterisk indicates a chelation site through the corresponding oxygen atom. $\Delta\delta_{exp,th} = \delta_{exp} - \delta_{th}$. a, b, c, d, e, and f are respectively the aligning of complex models of Figure 5.

A good correlation is observed between the performed calculation of ^{13}C NMR chemical shifts for complex 1 and the experimental values observed for complex A. This model features a ditungstate ion chelated to mannose in its β-furanose form involving a tetradentate O1,2,3,5 binding site in which O2,5 are the bridging oxygen atoms (**complex 1, *Figure S6*** in the **Supporting Information**). Both tungsten WO_6 octahedra share a face. This species was already discussed in the literature for which the carbon chemical shifts agree with the so-called complex L (***Table 1, Figure 1,a).***

The values computed for complex 3 match best with species B. Complex B thus involves a ditungstate center coordinated to the hydrated acyclic form of mannose in a tetradentate fashion through O1,2,3,4 oxygen donor site in a sickle arrangement, where O1,3 are bridging atoms with the two WO_6 octahedra sharing a face ***(*complex 3*, Figure S7*** in the **Supporting Information*)***. The current species was already discussed in the literature but only for molybdate complexes. Bilik and co-workers proposed dimolybdate complexes for mannose epimerization comprising the hydrated sugar chelating the metallic ion by its O1,2,3,4 deprotonated hydroxyl groups in a sickle arrangement.[12,32] Such observation reveals the possibility of tungsten to catalyze the epimerization of sugars the same way molybdenum does.

As for complex C, the comparison is more ambiguous since all the calculated chemical shifts of the proposed models differ more strongly than for the other complexes from the experimental values. However, the chemical shifts detected for complex C match with the species denoted M in the literature (***Table 1).*** This complex forms a ditungstate center chelated to α-mannofuranose in which four donor non vicinal hydroxyl groups (ring O2,3 and side chain O5,6) constitute the site of chelation. Among all the proposed models complex 7 shows the best correlation with species C. This complex involves a chelation site identical to the M type complex from previous work, consisting of four oxygen coordinated (O2,3,5,6) in which O3,5 are the bridging atoms (**complex 7*, Figure S8*** in the **Supporting Information**).

The ^{13}C NMR chemical shifts displayed for complex 11 match the most with the experimental chemical shifts reported for complex D. Complex D includes a monomeric tungstate ion chelated to α-mannofuranose through a monodentate site by deprotonation of second hydroxyl group (***Figure S9*** in the **Supporting Information**).

Focusing on the models built on the basis of an AMT structure, complex 13 involving β-mannofuranose as a ligand approximately correlates with the experimental chemical shifts displayed by complex A and the values calculated for the dimeric model (complex 3). Complexes 14 and 15, proposed respectively as models for complexes B and C, showed a large deviation from the experiments, thus, they were not retained as proper candidates. However, our analysis of the speciation as presented on Figure 3 clearly indicates that Complexes A and B may not have a nuclearity higher than 3, thus AMT itself might not be suited for the formation of complexes. However, this does not fully exclude the presence of a species of nuclearity higher than two.

Hence the final structures of the four species are illustrated in ***Figure 6***, obtained from the multi-technique method combining ^{13}C, ^{13}C-^{1}H, ^{1}H-^{1}H NMR, XANES and DFT. Out of these species, two correspond to previous proposals (***Figure 1***), but the two other ones have never been observed for tungsten-sugar systems.

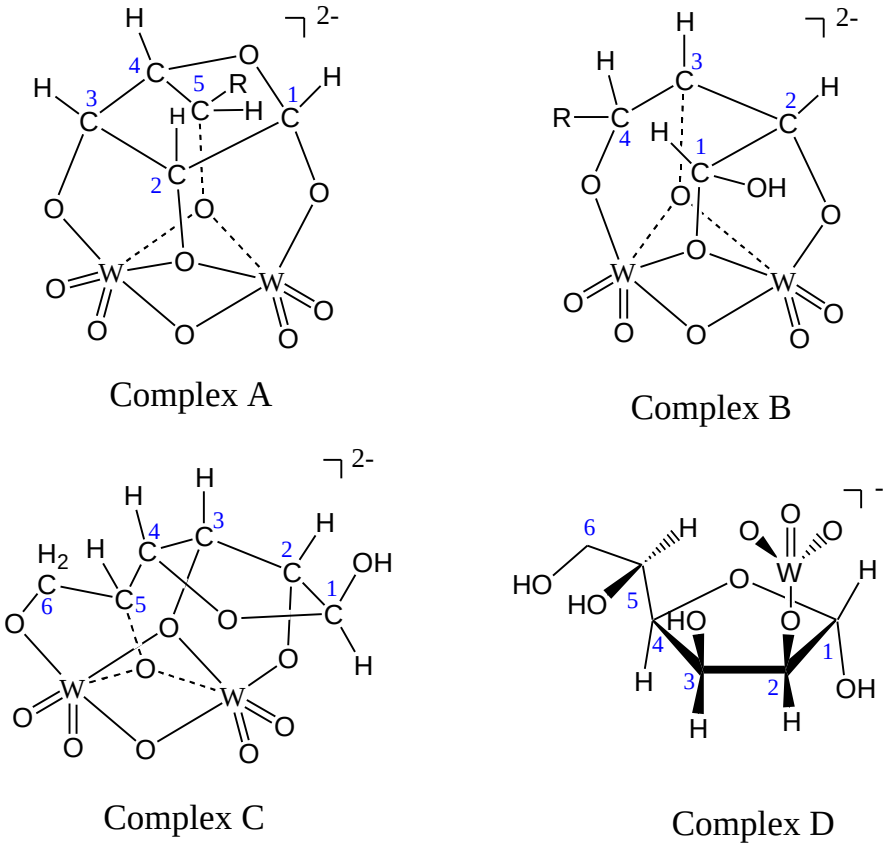

Figure 6. *Final structures for complexes A, B, C and D . R= CH_2OH in A, $CHOH\text{-}CH_2OH$ in B.*

Finally, we represent on **Figure 7** the comparison between the aqueous phase speciation of tungstate ions in the absence of mannose as simulated by the Medusa software with the speciation of mannose-tungsten complexes determined by this study, for a similar total concentration of tungsten ions of 1.0 mol L^{-1}. We find that the two types of speciation share some similarities, with species of low nuclearity only existing at high pH values and multi-nuclear species existing at medium pH. However, some features are clearly distinct, among which (i) the limit of the multi-nuclear/mononuclear domains is shifted to somewhat higher pH values in the presence of mannose (from around 7.5 to around 9) (ii) no complex whatsoever of mannose could be detected at pH values lower than around 3.5, despite the existence of polynuclear species of W in aqueous solutions at such concentrations and pH. These observations clearly show that the formation of the complexes between mannose and tungsten

does not involves a simple ligand-metal bond formation only, but a full redistribution of the tungsten nuclei and displacement of the equilibria at stake, and thus the speciation of mannose-tungsten (and likely more generally sugars-tungsten) cannot be merely inferred from that of the tungsten oxyanions in aqueous solution.

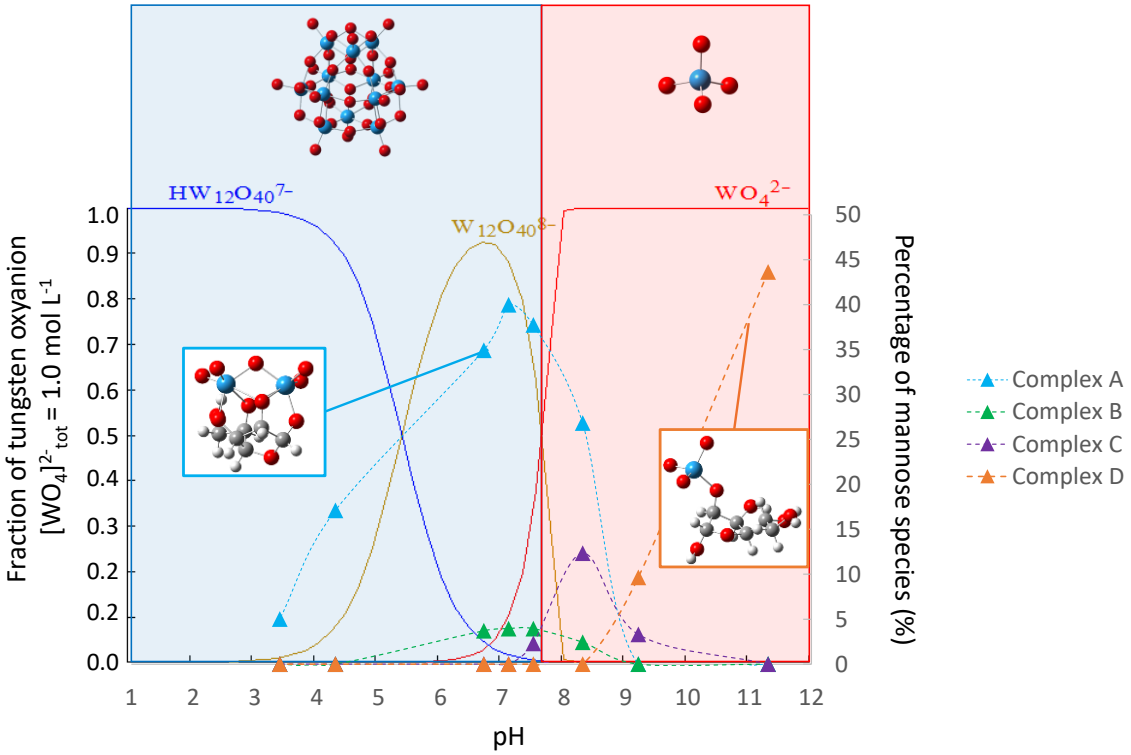

Figure 7. *Comparison of the aqueous-phase speciation of tungsten oxyanions in the absence of mannose, as simulated by the Medusa software for a total concentration of tungsten of 1.0 mol L^{-1} (solid lines, left axis) and of the speciation of the complexes between mannose and tungsten as determined in this study (experimental datapoints with dashed lines, right axis).*

Conclusion

In the present work, we examined the complexation of mannose with tungstate oxyanions potentially involved in important sugar conversion reactions, such as epimerization and retro-aldolization. We used a combination of spectroscopic (^{13}C, ^{13}C-^{1}H, ^{1}H-^{1}H NMR and XAS spectroscopy) and computational methodologies (DFT calculations) to propose molecular models of these complexes. We find a series of 4 distinct complexes, all of which were found of W^{6+} oxidation state (XANES). We showed that the existence of species involving the

aldehyde form of mannose are very unlikely. The complexes are characterized by different chemical structures of both the sugar and the metal core. In particular, we could distinguish two species dominant at neutral pH likely featuring a dinuclear tungsten core (even if our results do not fully exclude higher nuclearity, although not higher than 3 W atoms) with mannose in either a furanose form (major species) or linear hydrate form (minor species). As the pH increases, two additional complexes are observed as the two other ones vanish: a species essentially observed at pH 8-9, still involving a polynuclear metallic core, and finally at pH higher than 10, one mononuclear complex featuring a tungstate core in a tetrahedral environment and the α-furanose form of mannose. Note that all of these species involve the coordination of the hydroxyl in second position, which is reminiscent of a recent finding that the coordination of the β-hydroxyl group is mandatory for the promotion of C-C cleavage reactions by tungsten trioxide surface in a recent study[31] – although only complexes involving the carbonyl group were modelled where we could not observe any.

Overall, our result show that the speciation of W-mannose complexes qualitatively parallels the speciation of W oxyanions in aqueous solutions, with mononuclear, tetrahedral species at high pH (> 9) and polynuclear octahedral species in neutral solutions (3 < pH < 8). However, the maximum nuclearity is significantly different, with W_{12} oligomers in the absence of sugar and at most 3 in the presence of mannose). The boundaries in terms of pH also slightly vary, although not that much. Hence, the presence of sugars not only leads to the formation of complexes, but also strongly displaces the equilibria between the tungsten species in solution. Thus, our results shed new light on the speciation of complexes between sugars and tungsten and will be helpful to decipher the relationships between reaction conditions and catalytic activity in future works.

Supporting Information

Additional information concerning D-mannose conformation are present. Computational details regarding the choice of the proper functional/basis set combination for ^{13}C NMR are available along with the structures of all the proposed complexes in this manuscript. Additional NMR data (CIS value calculation) are provided.

Author Information

Corresponding Author

Dr. Kim Larmier *- IFP Energies Nouvelles, Rond-Point de l'Echangeur de Solaize, 69360 Solaize, France ; Email : kim.larmier@ifpen.fr*

Author Contributions

The manuscript was written through contribution of all authors. All authors have given approval to the final version of the manuscript.

Acknowledgments

The authors acknowledge the European Synchrotron Radiation Facility (ESRF) (Grenoble, France) and the CRG-FAME BM30 beamline (French Absorption spectroscopy beamline in Material and Environmental science) staff for the XAS experiments.

References

(1) Tursi, A. A review on biomass: importance, chemistry, classification, and conversion. *Biofuel Res. J.* **2019**, *6* (2), 962–979. DOI: 10.18331/BRJ2019.6.2.3.

(2) Zeikus, J. G.; Jain, M. K.; Elankovan, P. Biotechnology of succinic acid production and markets for derived industrial products. *Applied Microbiology and Biotechnology* **1999**, *51*, 545–552.

(3) Lam, E.; Chong, J. H.; Majid, E.; Liu, Y.; Hrapovic, S.; Leung, A. C.; Luong, J. H. Carbocatalytic dehydration of xylose to furfural in water. *Carbon* **2012**, *50* (3), 1033–1043. DOI: 10.1016/j.carbon.2011.10.007.

(4) Liu, X.; Wang, X.; Yao, S.; Jiang, Y.; Guan, J.; Mu, X. Recent advances in the production of polyols from lignocellulosic biomass and biomass-derived compounds. *RSC Adv* **2014**, *4* (90), 49501–49520. DOI: 10.1039/C4RA06466F.

(5) Wilson, K.; Lee, A. F. Bio-based chemicals from biorefining: carbohydrate conversion and utilisation. In *Advances in Biorefineries*; Elsevier, 2014; pp 624–658. DOI: 10.1533/9780857097385.2.624.
(6) Zhang, Z.; Huber, G. W. Catalytic oxidation of carbohydrates into organic acids and furan chemicals. *Chemical Society reviews* **2018**, *47* (4), 1351–1390. DOI: 10.1039/c7cs00213k.
(7) Sajid, M.; Farooq, U.; Bary, G.; Azim, M. M.; Zhao, X. Sustainable production of levulinic acid and its derivatives for fuel additives and chemicals: progress, challenges, and prospects. *Green Chem.* **2021**, *23* (23), 9198–9238. DOI: 10.1039/D1GC02919C.
(8) Istasse, T.; Richel, A. Mechanistic aspects of saccharide dehydration to furan derivatives for reaction media design. *RSC advances* **2020**, *10* (40), 23720–23742. DOI: 10.1039/d0ra03892j. Published Online: Jun. 22, 2020.
(9) *Avantium starts construction of bio-MEG demonstration plant in the Netherlands*. https://www.avantium.com/press-releases/avantium-starts-construction-of-bio-meg-demonstration-plant-in-the-netherlands/ (accessed 2023-03-16).
(10) Zheng, M.; Pang, J.; Sun, R.; Wang, A.; Zhang, T. Selectivity Control for Cellulose to Diols:Dancing on Eggs. *ACS Catal.* **2017**, *7* (3), 1939–1954. DOI: 10.1021/acscatal.6b03469.
(11) Yoo, C. G.; Li, N.; Swannell, M.; Pan, X. Isomerization of glucose to fructose catalyzed by lithium bromide in water. *Green Chem.* **2017**, *19* (18), 4402–4411. DOI: 10.1039/C7GC02145C.
(12) Bilik, V.; Matulova, M. Reactions of saccharides catalyzed by molybdate ions XLII. Epimerization and the molybdate complexes of aldoses. *Chemical Papers* **1990**, *44*, 257–265.
(13) Liu, Y.; Luo, C.; Liu, H. Tungsten trioxide promoted selective conversion of cellulose into propylene glycol and ethylene glycol on a ruthenium catalyst. *Angewandte Chemie (International ed. in English)* **2012**, *51* (13), 3249–3253. DOI: 10.1002/anie.201200351. Published Online: Feb. 24, 2012.
(14) Sun, R.; Wang, T.; Zheng, M.; Deng, W.; Pang, J.; Wang, A.; Wang, X.; Zhang, T. Versatile Nickel–Lanthanum(III) Catalyst for Direct Conversion of Cellulose to Glycols. *ACS Catal.* **2015**, *5* (2), 874–883. DOI: 10.1021/cs501372m.
(15) Deng, T.; Liu, H. Promoting effect of SnOx on selective conversion of cellulose to polyols over bimetallic Pt–SnOx/Al2O3 catalysts. *Green Chem* **2013**, *15* (1), 116–124. DOI: 10.1039/C2GC36088H.
(16) Tai, Z.; Zhang, J.; Wang, A.; Pang, J.; Zheng, M.; Zhang, T. Catalytic conversion of cellulose to ethylene glycol over a low-cost binary catalyst of Raney Ni and tungstic acid. *ChemSusChem* **2013**, *6* (4), 652–658. DOI: 10.1002/cssc.201200842. Published Online: Mar. 4, 2013.
(17) Sun, R.; Zheng, M.; Pang, J.; Liu, X.; Wang, J.; Pan, X.; Wang, A.; Wang, X.; Zhang, T. Selectivity-Switchable Conversion of Cellulose to Glycols over Ni–Sn Catalysts. *ACS Catal.* **2016**, *6* (1), 191–201. DOI: 10.1021/acscatal.5b01807.
(18) Komesu, A.; Rocha de Oliveira, Johnatt Allan; Da Silva Martins, L. H.; Wolf Maciel, M. R.; Maciel Filho, R. Lactic acid production to purification : a review. *BioResources* **2017**, *12* (2), 4364–4383.
(19) Zheng, M.; Pang, J.; Sun, R.; Wang, A.; Zhang, T. Selectivity Control for Cellulose to Diols: Dancing on Eggs. *ACS Catal.* **2017**, *7* (3), 1939–1954. DOI: 10.1021/acscatal.6b03469.
(20) Lis, H.; Sharon, n. Lectins: Carbohydrate-specific proteins that mediate cellular recognition. *Chemical reviews* **1998**, *98*, 637–674.
(21) Sears, P.; Wong, C.-H. Carbohydrate Mimetics: A New Strategy for Tackling the Problem of Carbohydrate-Mediated Biological Recognition. *Angew. Chem. Int. Ed.* **1999**, *38* (16), 2300–2324. DOI: 10.1002/(SICI)1521-3773(19990816)38:16<2300:AID-ANIE2300>3.0.CO;2-6.

(22) Yang, G.; Pidko, E. A.; Hensen, E. J. M. The mechanism of glucose isomerization to fructose over Sn-BEA zeolite:A periodic density functional theory study. *ChemSusChem* **2013**, *6* (9), 1688–1696. DOI: 10.1002/cssc.201300342.
(23) Chethana, B. K.; Mushrif, S. H. Brønsted and Lewis acid sites of Sn-beta zeolite, in combination with the borate salt, catalyze the epimerization of glucose:A density functional theory study. *Journal of Catalysis* **2015**, *323*, 158–164. DOI: 10.1016/j.jcat.2015.01.008.
(24) Montejo-Valencia, B. D.; Curet-Arana, M. C. Periodic DFT Study of the Opening of Fructose and Glucose Rings and the Further Conversion of Fructose to Trioses Catalyzed by M-BEA (M = Sn, Ti, Zr, or Hf). *J. Phys. Chem. C* **2019**, *123* (6), 3532–3540. DOI: 10.1021/acs.jpcc.8b10211.
(25) Yang, L.; Tsilomelekis, G.; Caratzoulas, S.; Vlachos, D. G. Mechanism of Brønsted acid-catalyzed glucose dehydration. *ChemSusChem* **2015**, *8* (8), 1334–1341. DOI: 10.1002/cssc.201403264.
(26) Yang, G.; Zhu, C.; Zhou, L. Adsorption of Glucose within M(IV)-Incorporated Zeolites:Insights from Periodic Density Functional Theory Calculations. *ChemistrySelect* **2016**, *1* (21), 6834–6840. DOI: 10.1002/slct.201601562.
(27) Yang, G.; Li, X.; Zhou, L. Adsorption of fructose in Sn-BEA zeolite from periodic density functional calculations. *RSC Adv.* **2016**, *6* (11), 8838–8847. DOI: 10.1039/C5RA25554F.
(28) Pidko, E. A.; Degirmenci, V.; van Santen, R. A.; Hensen, E. J. M. Coordination properties of ionic liquid-mediated chromium(II) and copper(II) chlorides and their complexes with glucose. *Inorganic Chemistry* **2010**, *49* (21), 10081–10091. DOI: 10.1021/ic101402r.
(29) Chethana, B. K.; Lee, D.; Mushrif, S. H. First principles investigation into the metal catalysed 1,2 carbon shift reaction for the epimerization of sugars. *Journal of Molecular Catalysis A: Chemical* **2015**, *410*, 66–73. DOI: 10.1016/j.molcata.2015.09.004.
(30) Stewart, C. D.; Arman, H.; Bawazir, H.; Musie, G. T. Synthesis, characterization, and spectroscopic investigation of new iron(III) and copper(II) complexes of a carboxylate rich ligand and their interaction with carbohydrates in aqueous solution. *Inorganic Chemistry* **2014**, *53* (20), 10974–10988. DOI: 10.1021/ic501351a. Published Online: Oct. 9, 2014.
(31) Liu, Y.; Zhang, W.; Hao, C.; Wang, S.; Liu, H. Unveiling the mechanism for selective cleavage of C-C bonds in sugar reactions on tungsten trioxide-based catalysts. *Proceedings of the National Academy of Sciences of the United States of America* **2022**, *119* (34), e2206399119. DOI: 10.1073/pnas.2206399119. Published Online: Aug. 19, 2022.
(32) Matulova, M.; Verchère, J.-F.; Chapelle, S. Furanose vs. acyclic forms of carbohydrate ligands. A multinuclear NMR spectroscopy of the molybdate and tungstate complexes of D-glycero-L-manno-heptose. *Carbohydrate research* **1996**, *287*, 37–48.
(33) De, S.; Dutta, S.; Patra, A. K.; Rana, B. S.; Sinha, A. K.; Saha, B.; Bhaumik, A. Biopolymer templated porous TiO2: An efficient catalyst for the conversion of unutilized sugars derived from hemicellulose. *Applied Catalysis A: General* **2012**, *435-436*, 197–203. DOI: 10.1016/j.apcata.2012.06.002.
(34) Jia, S.; He, X.; Xu, Z. Valorization of an underused sugar derived from hemicellulose: efficient synthesis of 5-hydroxymethylfurfural from mannose with aluminum salt catalyst in dimethyl sulfoxide/water mixed solvent. *RSC Adv.* **2017**, *7* (62), 39221–39227. DOI: 10.1039/C7RA07803J.
(35) Wilbur, D. J.; Williams, C.; Allerhand, A. Detection of the furanose anomers of D-mannose in aqueous solution. Application of carbon-13 nucelar magnetic resonance spectroscopy at 68 MHz. *Journal of the American Chemical Society* **1977**, *99*, 5450–5452.
(36) Hur, H.; Reeder, R. J. Tungstate sorption mechanisms on boehmite: Systematic uptake studies and X-ray absorption spectroscopy analysis. *Journal of colloid and interface science* **2016**, *461*, 249–260. DOI: 10.1016/j.jcis.2015.09.011. Published Online: Sep. 5, 2015.

(37) Chapelle, S.; Verchère, J.-F. Tungstate complexes of aldoses and ketoses of the lyxo series. Multinuclear NMR evidence for chelation by one or two oxygen atoms borne by the side chain of the furanose ring. *Carbohydrate research* **1995**, *277*, 39–50.
(38) Chapelle, S.; Verchère, J.-F. Tungsten-183 NMR studies of tungstate complexes of carbohydrates. 1. Characterization of two structural types in the alditol series. Evidence that the tungstate and molybdate threo complexes are not homologous. *Inorganic Chemistry* **1992**, *31*, 648–652.
(39) Chapelle, S.; Verchère, J.-F. A carbon-13 NMR study of the tungstate and molybdate complexes of perseitol, galacticol and mannitol. *Carbohydrate research* **1991**, *211*, 279–286.
(40) Shah, Z.; Geiger, M.; Al-Abed, Y.; Al-Tel, T. H.; Voetler; Wolfgang. Circular Dichroism of Carbohydrate-Molybdate Complexes. *Studies in Natural Products Chemistry* **1995**, *15*, 423–438.
(41) Taylor, G. E.; Waters, J. M. The structure of a compound of unexpected conformation involved in the xylose-lyxose epimerization. *Tetrahedron Letters* **1981**, *22*, 1277–1278.
(42) Bourne, E.; Hutson, D. H.; Weigel, H. Complexes between molybdate and acyclic polyhydroxy compounds. *Journal of the Chemical Society - Perkin Transaction* **1961**, 35–38.
(43) Chapelle, S.; Sauvage, J.-P.; Verchère, J.-F. 183W NMR Studies of Tungstate Complexes of Carbohydrates. 2. Competitive Formation of erythro and threo Complexes of Alditols. Characterization of a Novel Bis-Dinuclear Complex Formed with Perseitol. *Inorganic Chemistry* **1994**, *33*, 1966–1971.
(44) Da Silva, H. C.; Almeida, W. B. de. Theoretical calculations of 1H NMR chemical shifts for nitrogenated compounds in chloroform solution. *Chemical Physics* **2020**, *528*, 110479. DOI: 10.1016/j.chemphys.2019.110479.
(45) Semenov, V. A.; Samultsev, D. O.; Krivdin, L. B. The 1H and 13C NMR chemical shifts of Strychnos alkaloids revisited at the DFT level. *Magnetic resonance in chemistry : MRC* **2020**, *58* (6), 532–539. DOI: 10.1002/mrc.4948. Published Online: Nov. 24, 2019.
(46) Proux, O.; Nassif, V.; Prat, A.; Ulrich, O.; Lahera, E.; Biquard, X.; Menthonnex, J. J.; Hazemann, J. L. Feedback system of a liquid-nitrogen-cooled double-crystal monochromator: design and performances. *Journal of synchrotron radiation* **2006**, *13* (Pt 1), 59–68. DOI: 10.1107/S0909049505037441. Published Online: Dec. 22, 2005.
(47) Ravel, B.; Newville, M. ATHENA, ARTEMIS, HEPHAESTUS: data analysis for X-ray absorption spectroscopy using IFEFFIT. *Journal of synchrotron radiation* **2005**, *12* (Pt 4), 537–541. DOI: 10.1107/S0909049505012719. Published Online: Jun. 15, 2005.
(48) Tirado-Rives, J.; Jorgensen, W. L. Performance of B3LYP Density Functional Methods for a Large Set of Organic Molecules. *Journal of chemical theory and computation* **2008**, *4* (2), 297–306. DOI: 10.1021/ct700248k.
(49) Andersson, M. P.; Uvdal, P. New scale factors for harmonic vibrational frequencies using the B3LYP density functional method with the triple-zeta basis set 6-311+G(d,p). *The journal of physical chemistry. A* **2005**, *109* (12), 2937–2941. DOI: 10.1021/jp045733a.
(50) Frisch, M. J.; Trucks, G. W.; Schlegel, H. B.; Scuseria, G. E.; Robb, M. A.; Cheeseman, J. R.; Scalmani, G.; Barone, V.; Petersson, G. A.; Nakatsuji, H.; Li, X.; Caricato, M.; Marenich, A.; Bloino, J.; Janesko, B. G.; Gomperts, R.; Mennucci, B.; Hratchain, H. P.; Ortiz, J. V.; Izmaylov, A. F.; Sonnenberg, J. L.; Williams-Young, D.; Ding, F.; Lipparini, F.; Egidi, F.; Goings, J.; Peng, B.; Petrone, A.; Henderson, T.; Ranasinghe, D.; Zakrzewski, V. G.; Gao, J.; Rega, N.; Zheng, G.; Liang, W.; Hada, M.; Ehara, M.; Toyota, K.; Fukuda, R.; Hasegawa, J.; Ishida, M.; Nakajima, T.; Honda, Y.; Kitao, O.; Nakai, H.; Vreven, T.; Throssell, K.; Montgomery, J. A.; Peralta, J. E.; Ogliaro, F.; Bearpark, M.; Heyd, J. J.; Brothers, E.; Kudin, K. N.; Staroverov, V. N.; Keith, T.; Kobayashi, R.; Normand, J.; Raghavachari, K.; Rendell, A.; Burant, J. C.; Iyengar, S. S.; Tomasi, J.; Cossi, M.; Millam, J. M.; Klene, M.; Adamo, C.; Cammi, R.; Ochterski, J. W.; Martin, R. L.; Morokuma, K.;

Farkas, O.; Foresman, J. B.; Fox, D. J. *Gaussian 09, Revision B.01*; Gaussian, Inc., Wallingford CT, 2010.
(51) Laun, J.; Vilela Oliveira, D.; Bredow, T. Consistent gaussian basis sets of double- and triple-zeta valence with polarization quality of the fifth period for solid-state calculations. *Journal of computational chemistry* **2018**, *39* (19), 1285–1290. DOI: 10.1002/jcc.25195. Published Online: Feb. 22, 2018.
(52) Pritchard, B. P.; Altarawy, D.; Didier, B.; Gibson, T. D.; Windus, T. L. New Basis Set Exchange: An Open, Up-to-Date Resource for the Molecular Sciences Community. *Journal of chemical information and modeling* **2019**, *59* (11), 4814–4820. DOI: 10.1021/acs.jcim.9b00725. Published Online: Oct. 24, 2019.
(53) Weigend, F. Accurate Coulomb-fitting basis sets for H to Rn. *Physical chemistry chemical physics : PCCP* **2006**, *8* (9), 1057–1065. DOI: 10.1039/b515623h. Published Online: Jan. 3, 2006.
(54) Weigend, F.; Ahlrichs, R. Balanced basis sets of split valence, triple zeta valence and quadruple zeta valence quality for H to Rn: Design and assessment of accuracy. *Physical chemistry chemical physics : PCCP* **2005**, *7* (18), 3297–3305. DOI: 10.1039/b508541a. Published Online: Aug. 4, 2005.
(55) Marenich, A. V.; Cramer, C. J.; Truhlar, D. G. Universal solvation model based on solute electron density and on a continuum model of the solvent defined by the bulk dielectric constant and atomic surface tensions. *The journal of physical chemistry. B* **2009**, *113* (18), 6378–6396. DOI: 10.1021/jp810292n.
(56) Schreckenbach, G.; Ziegler, T. Calculation of NMR Shielding Tensors Using Gauge-Including Atomic Orbitals and Modern Density Functional Theory. *Journal of Physical Chemistry* **1995**, *99*, 606–611.
(57) Helgaker, T.; Jaszuński, M.; Ruud, K. Ab Initio Methods for the Calculation of NMR Shielding and Indirect Spinminus signSpin Coupling Constants. *Chemical reviews* **1999**, *99* (1), 293–352. DOI: 10.1021/cr960017t.
(58) Jayarathne, U.; Chandrasekaran, P.; Greene, A. F.; Mague, J. T.; DeBeer, S.; Lancaster, K. M.; Sproules, S.; Donahue, J. P. X-ray absorption spectroscopy systematics at the tungsten L-edge. *Inorganic Chemistry* **2014**, *53* (16), 8230–8241. DOI: 10.1021/ic500256a. Published Online: Jul. 28, 2014.
(59) Yamazoe, S.; Hitomi, Y.; Shishido, T.; Tanaka, T. XAFS Study of Tungsten L1- and L3-Edges: Structural Analysis of WO3 Species Loaded on TiO2 as a Catalyst for Photo-oxidation of NH3. *J. Phys. Chem. C* **2008**, *112* (17), 6869–6879. DOI: 10.1021/jp711250f.
(60) Chapelle, S.; Verchère, J. F. Tungstate complexes of aldoses and ketoses of the lyxo series. Multinuclear NMR Evidence For Chelation by One or Two Oxygen Atoms Borne by the Side Chain of the Furanose Ring. *Carbohydrate research* **1995**, *277*, 39–50.
(61) Eder, F.; Weil, M.; Schubert, W.-D.; Gierl-Mayer, C. Ammonium Metatungstate, (NH4)6[H2W12O40]: Crystallization and Thermal Behavior of Various Hydrous Species. *Crystal Growth & Design* **2021**, *21* (11), 6195–6212. DOI: 10.1021/acs.cgd.1c00639.
(62) Verchère, J.-F.; Sauvage, J.-P.; Rapaumbya, G.-R. Comparative study of various polyols as complexing agents for the acidimetric titration of tungstate. *Analyst* **1990**, *115*, 637–640.